

# Variable Augmented Network for Invertible MR Coil Compression

Xianghao Liao, Shanshan Wang, Lanlan Tu, Yuhao Wang, Dong Liang, *Senior Member, IEEE*,  
Qiegen Liu, *Senior Member, IEEE*

**Abstract**—A large number of coils are able to provide enhanced signal-to-noise ratio and improve imaging performance in parallel imaging. As the increasingly grow of coil number, however, it simultaneously aggravates the drawbacks of data storage and reconstruction speed, especially in some iterative reconstructions. Coil compression addresses these issues by generating fewer virtual coils. In this work, a novel variable augmented network for invertible coil compression (VAN-ICC) is presented, which utilizes inherent reversibility of normalizing-flow-based models, for better compression and invertible recovery. VAN-ICC trains invertible network by finding an invertible and bijective function, which can map the original image to the compression image. In the experiments, both fully-sampled images and under-sampled images were used to verify the effectiveness of the model. Extensive quantitative and qualitative evaluations demonstrated that, in comparison with SCC and GCC, VAN-ICC can carry through better compression effect with equal number of virtual coils. Additionally, its performance is not susceptible to different number of virtual coils.

**Index Terms**—Coil compression, Inverse network, Auxiliary variables, K-space, Deep learning.

## I. INTRODUCTION

Parallel imaging (PI) [1,2] can be mainly divided into three categories: parallel imaging in image domain, parallel imaging in k-space domain and parallel imaging in mixed domain, has been proposed during the past two decades to accelerate data acquisitions in magnetic resonance imaging (MRI). Parallel imaging (PI) [1-3] employs receiver arrays with multiple coils [4] to simultaneously acquire data. The different coil sensitivities of the receiver coils are applied to partially replace traditional k-space encoding and reduce scan time. With the growing development of parallel imaging (PI), MRI data acquisitions have been significantly accelerated. This has caused many lengthy MR exams clinically feasible. In addition to PI, there is a growing trend towards utilizing constrained reconstructions in MRI, such as compressed sensing (CS) [5]. However, these reconstructions are often iterative and therefore much more computationally intensive. What's more, these techniques use prior information to achieve superior image quality, enhanced resolution and elevated signal-to-noise ratio (SNR). Higher accelerations in data acquisition can be achieved by combining CS with PI [6-8]. Coil arrays [3] is essential for PI methods and the quality of the PI results lies

on the number and arrangement of the independent coil elements. The large coil arrays are able to provide high signal-to-noise ratio (SNR) and enhance PI performance. With the lever of hardware technology improving, many researches apply large coil arrays with up to even 128 independent receiver channels [4-7]. As the number of channels increasing, however, the MRI reconstruction speed and data storage drawbacks of these large datasets are becoming more prominent.

In order to reduce the computational cost for large coil arrays [3,8,9] and fulfill improved data processing efficiency in the large array systems, the method of coil compression [8-11] has been proposed. The essence of coil channel compression technology is to linearly combine raw data from multiple coil channels into specific virtual coil channel [8] data or to select the most considerable set of data from all virtual coil channel data to reduce the number of coil channel data received independently before image reconstruction is totally completed. At the same time, coil channel compression technology is capable of significantly reducing the reconstruction time, because the amount of computations for constrained and PI reconstruction is determined by the number of coil channels. Furthermore, the coil channel compression algorithm can reduce the number of virtual coil channels while retaining as many available signals as possible.

In general, coil compression methods can be classified as the kinds of hardware and software compression. Coil channel compression was initially applied to hardware. Using the theoretical knowledge of the noise covariance of the receiver array, the original multiple original coils are linearly combined into fewer eigen coils. King et al. [11,12] implemented an efficient coil compression method by combining coil array elements (in hardware) into an alternative basis set with zero noise correlation between array elements. This SNR-preserving data compression method advantageously allows users of MRI systems with fewer receiver channels to achieve the SNR of higher-channel MRI systems. Although the hardware implementation has SNR benefits, it is not always optimal because of not taking the spatial coil sensitivity variation or the received data into account, hence the hardware compression will cause a certain loss and we can't get the best image signal.

Comparing with hardware compression, software compression is more flexible and results in less losses. Buehrer et al. [9] proposed a means that achieving coil compression by optimizing SNR of region of interest in reconstruction image. It not only depends on the sensitivity of the coil and the accuracy of the sensitivity map, but also requires undersampling to produce a simple point spread function for practical point. Therefore, it is only suitable for sensitivity-based PI reconstructions such as SENSE [1]. Huang et al. [8] developed a different approach to reduce the size of PI data by employing principal component analysis (PCA) [13-15] in the k-domain, avoiding the need for coil sensi-

This work was supported in part by the National Natural Science Foundation of China under 61871206. Xianghao Liao is the first authors. (Corresponding authors: Qiegen Liu.)

Xianghao Liao, Lanlan Tu, Yuhao Wang and Qiegen Liu are with the Department of Electronic Information Engineering, Nanchang University, Nanchang 330031, China. ({liaoxianghao, lanlantu}@email.ncu.edu.cn, {wangyuhao, liuqiegen}@ncu.edu.cn)

tivities and noise covariance. Feng *et al.* [16] presented a method to reduce the computation cost in the k-domain PI, by utilizing the fact that in large arrays the channel sensitivity is localized to calculate the cross-channel correlation for channel selection. Zhang *et al.* [3] performed separately for each location along the fully sampled dimensions, which was based on a singular value decomposition (SVD), to compress data in a hybrid image-k-domain. Beatty *et al.* [17] devoted to a new approach that combines the k-space reconstruction kernel with a coil compression kernel, which is similar to generalized auto calibrating partially parallel acquisitions-based simultaneous-multi slice-acquired coil compression (GRABSMACC), because its unaliasing process is also responsible for coil compression. Doneva *et al.* [18] raised a new method of correlation with coil sensitivity information, in which the optimal subset of receiving coil channels is determined by the contribution of each coil channel to the final reconstructed image. Liu *et al.* [19,20] took sparse magnetic resonance into consideration, combining SENSE algorithm in the meanwhile. The reconstruction way is named as Sparse-SENSE, which owns a good final image effect and a high acceleration ratio.

The single coil channel compression algorithm (SCC) [8] and the geometric decomposition coil channel compression algorithm (GCC) [3] are both traditional software compression algorithms, which are of high reference value with a long history. Both SCC and GCC require two main steps to achieve coil compression. The first step is to find a suitable coil compression matrix; the second step is to apply the coil compression matrix to the original coil and construct a virtual coil. Besides, they are able to obtain image quality comparable to that are acquired from all original coil channel data reconstruction. In the same situation, all indexes of GCC are better than SCC. The compression loss of GCC is smaller than that of SCC. In order to achieve similar errors as in GCC, more virtual coils are often demanded in SCC.

Following the success of deep learning in a wide range of applications, neural network-based machine learning techniques have received interest as a means of accelerating MRI. An idea is inspired by deep learning techniques, especially generative models from computer vision and image processing.

Inspired by the prior arts, for the first time, we employ a deep learning algorithm for magnetic resonance coil compression in this work. The novel and effective invertible coil compression method called VAN-ICC-K, taking advantage of the inherent reversibility of normalizing-flow-based models [21,22]. It is designed with the composition of a stack of affine coupling layers and it utilizes the invertible  $1 \times 1$  convolution as the learnable permutation function between the coupling layers. In the forward compression process, it designs the 12 channels to 4 channels in k-space mapping in our invertible model with one single invertible neural network. In particular, due to the model reversibility, our method also achieves reversible compression, namely recovering 4 channels to 12 channels image in k-space, comparing with other software and hardware compression methods. Moreover, unlike the natural image reversible compression, MR image compression need to handle the complicated complex value. The experimental results indicate that VAN-ICC-K can not only significantly compress but also recover nearly perfect quality 12-channel MRI from compressed 4-channel images in k-space. In addition, because the coil compression is performed in k-space, this

approach is not susceptible to tight imaging field-of-view (FOV) artifacts. VAN-ICC-I is a method we have previously proposed to perform image compression directly in the image domain. The VAN-ICC-K method is a qualitative leap forward from the VAN-ICC-I method in that it shifts the compression scenario from the image domain to k-space, which is more realistic and feasible for hospitals when collecting data, increasing the possibility of applying the method to real-life situations.

The major contributions of this study are as follows:

- Our previous work has been successfully recruited at conference. Building on previous work, we have undertaken additional substantial extensions and in-depth studies, introducing the concept of k-space and applying coil compression in the k-space domain.
- Our framework leverages the core idea from the perspective of invertible neural networks to compress and recover multi-coils images, which can address the issue of information loss in coil compression procedure.
- Auxiliary variables technology is adopted to make the channel number of the network output to be equal to the network input, and implicitly reduces the coil dimension.
- The proposed method VAN-ICC can always achieve excellent compression result, and its performance is insensitive to the number of different virtual coils, compared with the other methods.

The rest of this paper is presented as follows. In Section II, we briefly describe some relevant works on coil compression, the invertible model and affine coupling layer. Proposed method (VAN-ICC), optimization function and network structure are introduced in Section III. Section IV plays a critical role in the paper. In this part, we conduct the major experiments. Section V concludes with topics and future works are given.

## II. RELATED WORK

### A. Overview of the Theory of Coil Compression

Before reconstructing the image,  $N < M$  with a series of linear combinations are performed in the time domain to reduce the amount of independent data flowing from the  $M$  coil input channels to the  $N$  coil output channels, where coil compression comes in. The following equation accurately represents the coil compression problem:

$$v'(k) = Av(k) \quad (1)$$

where  $v(k)$  denotes a vector that encompasses the data from all  $n$  coils at k-space location  $k$ .  $A$  is described as a matrix with dimension  $M \times N$  and it is able to be solved by PCA in data-based coil compression [8].  $v'(k)$  demonstrates the data vector from virtual coils that the size reduces from  $M$  to  $N$ .

An approximate representation of the original coil can be achieved by a proper linear combination of virtual coils:

$$v(k) = A^H v'(k) + \varepsilon \quad (2)$$

where  $A^H$  is conjugate transpose matrix of  $A$ , and  $\varepsilon$  stands for the approximate error.

How to minimize the coil compression error with a fixed number of virtual coils is the essence of the coil compression problem

$$\min_A \sum_k \| (A^H A - I) v(k) \|^2 \quad (3)$$

$$s.t. AA^H = I$$

The solution for Eq. 3 can also be obtained by PCA or SVD.

### B. Invertible Neural Networks

In the previous section, coil compression methods simply compressed the input linearly, which is not the case with neural networks, which often have to map the input non-linearly. Nowadays, one of the popular choices in solving image generation tasks is flow-based invertible neural networks [21-24], whose network structure is in principle reversible, but whose inverse process is computationally expensive and cannot really be used in our daily lives. NICE [23] and RealNVP [21] presented that using couple layers can make fully invertible networks a natural choice. NICE [23] is the first learning-based normalizing flow framework with the proposed additive coupling layers. RealNVP [21] combines additive and multiplicative coupling layers together to be a general "affine coupling layer", and successfully introduces a convolutional layer in the coupling model, which making it possible to better deal with image problems. The Glow algorithm proposed by Kingma [22] incorporates invertible  $1 \times 1$  convolutions into affine coupling layer and achieves linearly combine dimensions of the data. Flow++ [24] used the logistics mixture CDF (cumulative distribution function) coupling flows instead of affine coupling layer and employed purely convolutional conditioning networks in coupling layers.

### C. Affine Coupling Layer

True invertible neural networks are typically constructed using coupling layers [21-23]. NICE [23] and RealNVP [21] presented coupling layers with a normalizing flow by stacking a sequence of invertible bijective transformation functions. The bijective function is designed as an affine coupling layer, which is a tractable form of Jacobian determinant, and both forward and inverse function are efficiently computable. In our case, we use an affine coupling layer [21], it mainly includes three steps.

Firstly, it will be more beneficial for us to train deeper networks in the Glow architecture [22], due to the fact that each bionic coupling layer performs a specific identity function in its initial state.

Secondly, the input involves all the channels and performs a concatenation and segmentation operation. It is worth noting that the segmentation function along the channel dimension first splits the input tensor into two and then concatenates them both into one tensor using latent variables of different scales. In this step, we choose to split the input tensor into three parts of exactly equal size along the channel dimension.

Finally, before each step, we perform a reversible convolution, which is done to improve the influence of each dimension on the other dimensions after enough flow steps. This will be discussed in detail in the next subsection.

### D. Invertible $1 \times 1$ Convolution

Following Glow's [22] approach, an invertible  $1 \times 1$  convolution is added before each affine coupling layer in order to better fuse the information carried by each part after segmentation and to prevent the problem that some channels may never be updated. It is worth noting that a single invertible  $1 \times 1$  convolution operation is performed, that is, channels with the same number of input and output channels

are swapped.

The log-determinant of an invertible  $1 \times 1$  convolution of a  $h \times w \times c$  tensor  $h$  with  $c \times c$  weight matrix  $W$  is straightforward to compute:

$$\log \left| \det \left( \frac{d\text{conv}2D(h; W)}{dh} \right) \right| = h \cdot w \cdot \log |\det(W)| \quad (4)$$

The cost of computing of differentiating  $\det(W)$  is  $O(c^3)$ , which is often comparable to the cost computing  $d\text{conv}2D(h; W)$  which is  $O(h \cdot w \cdot c^3)$ . We initialize the weights  $W$  as a random rotation matrix, having a log-determinant of 0; after one SGD step these values start to diverge from 0.

Thus, to make the Glow algorithm fast, using an LU-decomposition to calculate the matrix mentioned above. This cost of computing  $\det(W)$  can be reduced from  $O(c^3)$  to  $O(c)$  by parameterizing  $W$  directly in its LU decomposition:

$$W = PL(U + \text{diag}(s)) \quad (5)$$

where  $P$  is a permutation matrix,  $L$  is a lower triangular matrix with ones on the diagonal,  $U$  is an upper triangular matrix with zeros on the diagonal, and  $s$  is a vector. The log-determinant is then simply:

$$\log |\det(W)| = \text{sum}(\log |s|) \quad (6)$$

For large  $c$ , the difference between computational costs will become more significant, although this large difference in wall clock computing time is not reflected in the networks in which we conducted specific experiments.

In this parameterization, we initialize the parameters by first sampling a random rotation matrix  $W$ , then computing the corresponding value of  $P$  (which remains fixed) and the corresponding initial values of  $L$  and  $U$  and  $s$  (which are optimized).

## III. PROPOSED MODEL

### A. Proposed Method (VAN-ICC)

We define the forward process as mapping MR images of multiple coils to images of fewer coils. In addition to the forward process, a reverse process is also needed to restore the hidden features in the compressed images via the VAN-ICC method. In general, in classical neural networks, two completely independent networks are needed to perform these two processes, and this sometimes leads to the production of inaccurate biased mappings. Therefore, we take an alternative approach and implement network reversibility in a single network, which not only simplifies the structure of the network, but also makes training much simpler and easier.

We use the high-dimensional tensor  $X$  to denote the original data space and  $Y$  to represent the space used to compress the data. It is well known that a natural image is not a complex-valued image, but the MR image used in our experiments is complex-valued. Thus, in our experiment, the real and imaginary parts of the  $n$ -channel MR image are inevitably treated as two mutually independent channels, let  $X = \{[x_{\text{real}1}, x_{\text{imag}1}], \dots, [x_{\text{real}n}, x_{\text{imag}n}]\}$ . Theoretically, an  $n$ -channel image can also be transformed to a  $2n$ -channel image. Invertible and bijective function which is for mapping data points from the original data space to the compressed data space, denoted as  $f: X \rightarrow Y$ , the essence is

reversible coil compression. The bijection function  $f$  is constructed from a sequence of invertible and tractability of Jacobian determinant transformations:  $f = f_0 \circ f_1 \circ f_2 \circ \dots \circ f_k$  (k is the number of transformations). Such a sequence of reversible transformations is a normalizing flow. For a given input  $x$ , by means of a reversible transformation, we can obtain the compressed data  $y$  and vice versa

$$y = f_0 \circ f_1 \circ f_2 \circ \dots \circ f_k(x) \quad (7)$$

$$x = f_0^{-1} \circ f_1^{-1} \circ f_2^{-1} \circ \dots \circ f_k^{-1}(y) \quad (8)$$

As shown in Fig. 1, the invertible block  $f_i$  is implemented through affine coupling layers. In each affine coupling layer, the D-dimensional input tensor  $u$  is split into two unequal parts,  $u_{1:d}$  and  $u_{d+1:D}$  ( $d < D$ ), along the channel dimension. Also,  $d < D$ , the output  $v$  can be obtained by

$$v_{1:d} = u_{1:d} \quad (9)$$

$$v_{d+1:D} = u_{d+1:D} \odot \exp(s(u_{1:d})) + t(u_{1:d}) \quad (10)$$

where  $s$  and  $t$  represent scale and translation functions.  $\odot$  is element-wise multiplication. Note that the scale and translation functions are not necessarily invertible, and thus they are realized by a succession of several fully connected layers with leaky ReLU activations.

We reinforce [25] the coupling layer, in order to improve the representation studying ability of the architecture, the Eq. (9) is rewritten as

$$v_{1:d} = u_{1:d} + r(u_{d+1:D}) \quad (11)$$

where  $r$  can be arbitrarily complicated functions of  $u_{d+1:D}$ .

Accordingly, given the output  $v$ , the inverse step is easily expressed as

$$u_{d+1:D} = (v_{d+1:D} - t(v_{1:d})) \odot \exp(-s(v_{1:d})) \quad (12)$$

$$u_{1:d} = v_{1:d} + r(u_{d+1:D}) \quad (13)$$

Then, in order to replace the reverse permutation operation, which not only reverses the ordering of the channels but also simplifies the architecture, we insert an invertible  $1 \times 1$  convolution presented in [22] between affine coupling layers. It is worth noting that although 3-channel input cannot be even split completely, the invertible  $1 \times 1$  convolution ensures that unchanged components will be updated promptly in the next invertible block.

Moreover, we follow the implementation of [26] and disable batch normalization [27] and weight normalization used in [21]. In our experiment, we carry out the 12-channel MR image into 3, 4, 5 and 6 channels and the 20-channel MR image into 4, 5, 8 and 10 channels respectively. Using the example of 12 channels to 4 channels, the channel compression reversible process is described in detail below. For solving our image-to-image translation task, we directly learn the 12-channel to 4-channel mapping with implicitly modeling the latent distribution.

Since the invertible  $1 \times 1$  convolution input size of invertible neural networks must be equal to the output size. Thus, achieving coil compression, we use an implicated dimension reduction technique by introducing auxiliary variables proposed in [28], which constraining 12-channel to be 3 identical 4-channel images via samples training. Specifically, we take the original 12-channel MR images data as input, and three copies of the original four channel image are used as the target. Then, the three sets of images are aver-

aged to obtain a set of four-channel images, and finally the compressed MR image can be obtained after sum of squares (SOS) [29-31]. We also do an online gamma correction (i.e. without storing on disk) to original image data to compress the dynamic range for faster convergence speed. The detailed training process is shown in the Fig. 3.

### B. Optimization Function

Invertible networks can support us to simultaneously minimize loss on both the input and output domains [32], which will lead to more effective training results. In the VAN-ICC-K method, the forward channel is utilized to generate a 4-channel image and the reverse channel is tasked with recovering the original image. It is noteworthy that we employed two completely different loss functions for training forward and reverse pass. Moreover, we conduct bi-directional training with smooth  $L_1$  loss, which has better overall performance than  $L_2$  loss in terms of robustness and stability.

We optimize our VAN-ICC-K model by minimizing the total loss

$$L = \lambda \|f(x) - y\|_1^{\text{smooth}} + \|f^{-1}(y) - x\|_1^{\text{smooth}} \quad (14)$$

where  $\lambda$  is the hyper-parameter used to balance the accuracy between compressed and original images reconstruction. We set  $\lambda$  to 1 in our main experiments. Given  $d$ , which represents the error between predicted value and ground truth. The smooth  $L_1$  is defined as

$$\text{smooth}_{L_1}(d) = \begin{cases} 0.5d^2 & \text{if } |d| < 1 \\ |d| - 0.5 & \text{otherwise.} \end{cases} \quad (15)$$

Due to all experimental data is multi-coil, the final consequence is obtained by merging these coil reconstructed images with sum of squares (SOS). In the image domain, the forward pass loss is expressed as Eq. (16) and the forward pass loss is denoted as Eq. (17) in the k-space domain:

$$L_f = \arg \min \|sos(x) - sos(\hat{x}_c)\|_1^{\text{smooth}} \quad (16)$$

$$L_f = \arg \min \|sos(ifft(x)) - sos(ifft(\hat{x}_c))\|_1^{\text{smooth}} \quad (17)$$

where  $sos$  is defined as  $y = \sum_{k=1}^N |X_k|^2$ ,  $X_k$  is the complex-valued image from channel  $K$ ,  $N$  is the number of channels, and  $x$  and  $\hat{x}_c$  denote the ground truth and compressed images, respectively.

The reverse pass loss:

$$L_r = \arg \min \|x - \hat{x}\|_1^{\text{smooth}} \quad (18)$$

where  $\hat{x}$  denotes the recovered images.

### C. Network Structure

In this section, our neural network architecture will be introduced in detail. The network backbone called InvBlock, follows the Glow [22] which consists of invertible  $1 \times 1$  convolution, affine coupling layers. The blocks are depicted pictorially in Fig. 1. In the affine coupling layer, as shown in the right of Fig. 1, the input character is split into two halves along the channel dimension. F, G, and H are transformation equal to DenseBlock [33], which consists of five 2D convolution layers with filter size  $3 \times 3$ . Each layer learns a new set of feature maps from the previous layer. The size of the receptive field for the first four convolutional layers is  $3 \times 3$ , and stride is 2, followed by a rectified linear unit (ReLU)

[34-36]. The last layer is a  $3 \times 3$  convolution without ReLU. The purpose of LeakyReLU [37-39] layers is to refrain from

overfitting to the training set [18] and further increase non-linearity.

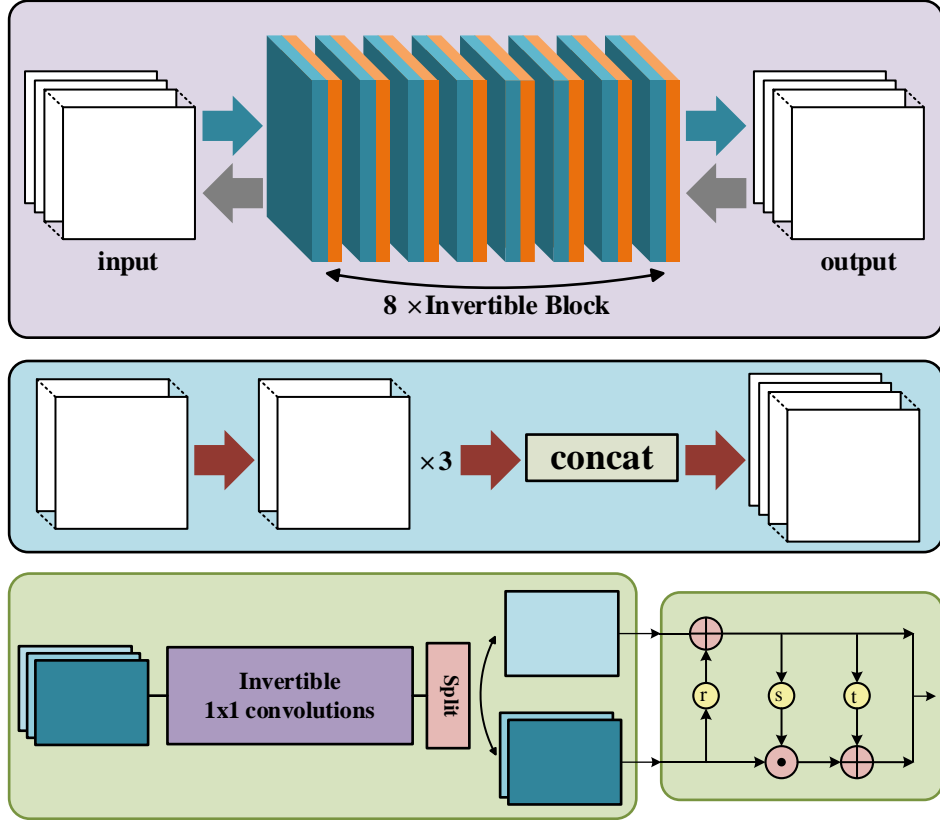


**Fig. 1.** Architecture framework of the proposed VAN-ICC. Top: description of network which has eight Invertible Block. Middle: the process of variable augmented strategy. Bottom: the structure of affine coupling layer.

## IV. EXPERIMENTS

### A. Experiment Setup

1) **Datasets:** In the experiments, we adopt two datasets to evaluate the VAN-ICC-I model and the VAN-ICC-K model. The training datasets are provided by Shenzhen Institutes of Advanced Technology, the Chinese Academy of Science.

Firstly, the brain data are scanned from a 3T Siemens's MAGNETOM Trio scanner by utilizing the T2-weighted turbo spin echo sequence. The relevant imaging parameters encompass the size of image acquisition matrix is  $256 \times 256$ , echo time (TE) is  $149\text{ ms}$ , repetition time (TR) is  $2500\text{ ms}$ , the field of view (FOV) is  $220 \times 220\text{ mm}^2$  and the slice thickness is  $0.86\text{ mm}$ . In addition, 480 MR images with 12-channel are employed as training data. In the meanwhile, 20 images are seen as validation data.

Secondly, 101 fully sampled cardiac MR images are acquired with T1-weighted FLASH sequences via taking advantage of 3T MRI scanner (SIMENS MAGNETOM Trio), whose slice thickness is  $6\text{ mm}$ . Typically, the TR/TE is  $5/3\text{ ms}$ ; acquisition matrix size is  $192 \times 192$ ; FOV is  $330 \times 330\text{ mm}^2$ , and the number of receiver coils is 24. The raw multi-coil data of each frame are combined by an adaptive coil combination method to generate a single-channel complex value image.

2) **Implementation Details:** In this work, we employ MR images as the network input. Notice that the input and output are all complex-valued images with the same size. Each includes real and imaginary components. The smooth  $L_1$  loss is adopted for training to compare with the ground truth in

the image domain. Adam optimizer is used to train the network. The size of mini batch is 1, and the number of epochs in single and multi-coil networks are 1000 and 500, respectively. The initial learning rate is  $10^{-5}$ , which gradually drops to half until 20 epochs. It is of significant worth to take note of the hyperparameters:  $\alpha$ , and  $\beta$  are the weights associated with different loss terms. The labels for the network are the images generated from direct Fourier inversion from fully sampled k-space data. The sampling in the Fourier domain utilizes Cartesian sampling strategy, whose accelerated factor is  $R = 3$ .

The proposed method is implemented in python, using Pytorch and Operator Discretization Library (ODL) interface [40] on 2 NVIDIA Titan XP GPUs, 12GB RAM. Training time lasts about 2 days and the source code is available at: <https://github.com/yqx7150/VAN-ICC>.

3) **Evaluation Metrics:** Compression and reconstruction results obtained by VAN-ICC-K are compared relatively to data reconstructed from all 12 coil elements in the original array. To quantitatively evaluate the quality of reconstructed images, we employ three image quality metrics, such as peak signal to noise ratio (PSNR) [41], structural similarity (SSIM) [41, 42] and high frequency error norm (HFEN) [43, 44].

The PSNR is defined by

$$PSNR = 20 \log_{10} \left( \frac{\text{Max}(x^*)}{\|x - x^*\|_2} \right) \quad (19)$$

where  $x$  and  $x^*$  denote the reconstructed and ground truth images, respectively.

The SSIM index is defined as:

$$SSIM = \frac{(2\mu_x\mu_{x^*} + c_1)(2\sigma_{xx^*} + c_2)}{(\mu_x^2 + \mu_{x^*}^2 + c_1)(\sigma_x^2 + \sigma_{x^*}^2 + c_2)} \quad (20)$$

where  $\mu_x$  is an average of  $x$ ,  $\sigma_x^2$  is a variance of  $x$  and  $\sigma_{xx^*}$  is a covariance of  $x$  and  $x^*$ . There are two variables to stabilize the division such as  $c_1 = (k_1 L)^2$  and

$c_2 = (k_2 L)^2$ .  $L$  represents for a dynamic range of the pixel intensities.  $k_1$  and  $k_2$  are constants by default  $k_1 = 0.01$  and  $k_2 = 0.03$ .

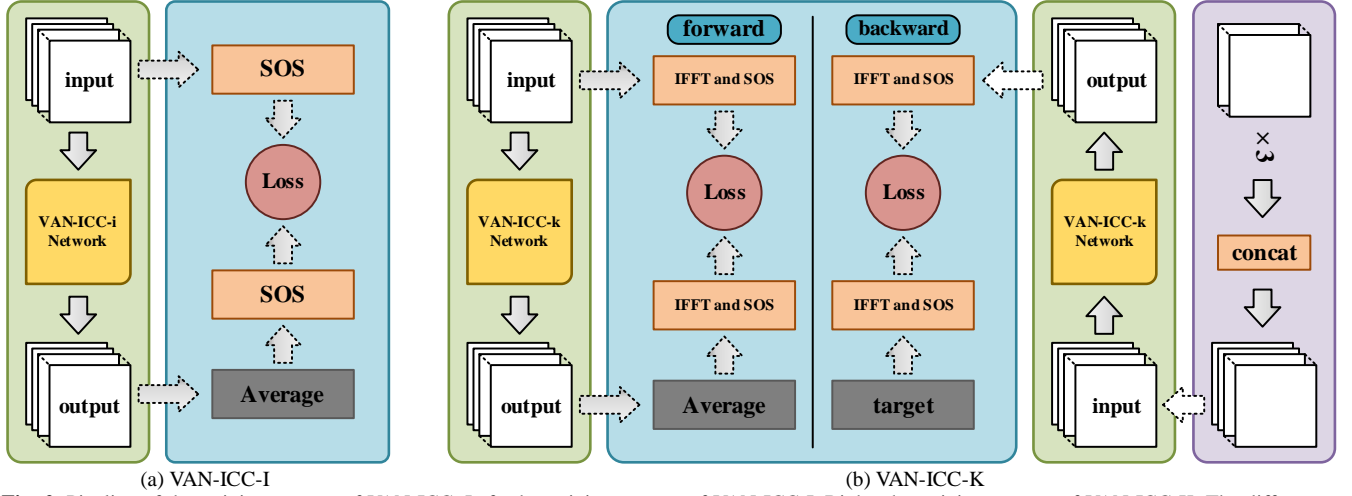


Fig. 2. Pipeline of the training process of VAN-ICC. Left: the training process of VAN-ICC-I. Right: the training process of VAN-ICC-K. The differences between VAN-ICC-I and VAN-ICC-K are the IFFT and SOS module and that the input and output of VAN-ICC-K are on k-space domain.

### B. Experiments on Image Domain

1) **Coil Compression of Fully Sampled Data:** In this experiment, the virtual coils are set to 4 and 10 for original 12-channel brain images and 20-channel cardiac images, respectively. Quantitative evaluation is placed in Table I. A comparison of image quality metrics for all compression methods demonstrated the superior performance of VAN-ICC-I. In the brain datasets, the average PSNR value of our method is higher than SCC and GCC by more than 10 and 8 dB, respectively. Moreover, the SSIM obtained by VAN-ICC-I is also the highest among the three methods. For Cardiac datasets, the PSNR of the introduced method reaches 55 dB. However, the SCC and GCC is only 31 dB and 36 dB. Besides, the SSIM of VAN-ICC-I is also highest.

TABLE I

QUANTITATIVE EVALUATION (PSNR/SSIM) RESULTS BY DIFFERENT METHODS IN THE TEST DATASETS.

Algorithm	SCC	GCC	VAN-ICC-I
Brain	41.53/ 0.9808	43.36/ 0.9820	<b>52.04/ 0.9993</b>
Cardiac	31.15/ 0.9760	36.64/ 0.9917	<b>55.33/ 0.9995</b>

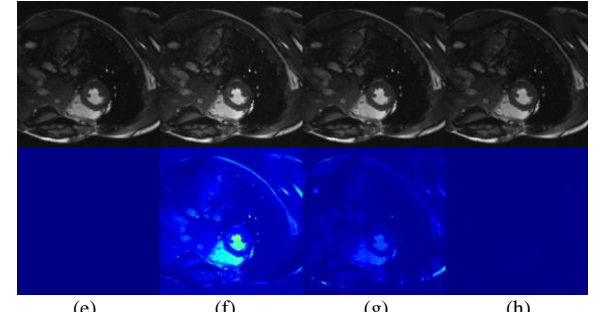
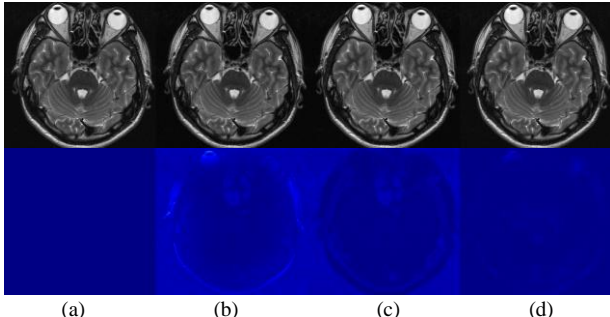


Fig. 3. Comparison of compression results on brain dataset and cardiac dataset for different methods. (top 2 rows: brain images, and bottom 2 rows: cardiac images) Top: (a) Reference image of brain dataset; (b) SCC-4ch; (c) GCC-4ch; (d) VAN-ICC-I-4ch; (e) Reference image of cardiac dataset; (f) SCC-10ch; (g) GCC-10ch; (h) VAN-ICC-I-10ch. Bottom: The 3 × absolute difference images between the reference images and compressed images of corresponding position.

Fig. 3 demonstrates the compression results of SCC, GCC and VAN-ICC-I in brain and cardiac datasets. Besides, the SOS image from 12 and 20 original coil are employed as reference, respectively. It is obvious that our method is able to generate realistic compressed images that closely resemble the original ground-truth images. Comparing with SCC and GCC, VAN-ICC-I maintains fine features in the edge details. Apart from that, it is most comparable in terms of qualitative visual quality. This is further indicated through the absolute difference maps where unlike the VAN-ICC-I method, SCC and GCC all have lower similarity around the edges or in the background.

2) **Compression for Different Virtual Coils:** To verify the robustness of the raised VAN-ICC-I, 12-channels brain images are chosen to be compressed into 6 and 4 virtual coils, respectively. Generally speaking, the smaller the number of virtual coils is, the worse the compression performance will be. Fortunately, as exhibited in Fig. 4, VAN-ICC-I is able to still achieve superior results in the circumstance of compressing into fewer virtual coils. As illustrated in Table 2, the

average PSNR value of the compressed images in GCC with 4 virtual coils decreases by 6 dB in comparison with the 6 virtual coils result. SCC also reduces 3 dB in the same case. By contrast, the PSNR value accomplished by VAN-ICC-I only descends by 0.24 dB, which is still effective frankly.

TABLE II  
QUANTITATIVE RECONSTRUCTION RESULTS FOR  
VAN-ICC, SCC AND GCC AT DIFFERENT VIRTUAL COILS.

Method	SCC	GCC	VAN-ICC-I
12ch $\rightarrow$ 6ch	46.27/0.9915	49.47/0.996	<b>52.28/0.9995</b>
12ch $\rightarrow$ 4ch	43.53/0.9808	43.36/0.982	<b>52.04/0.9993</b>

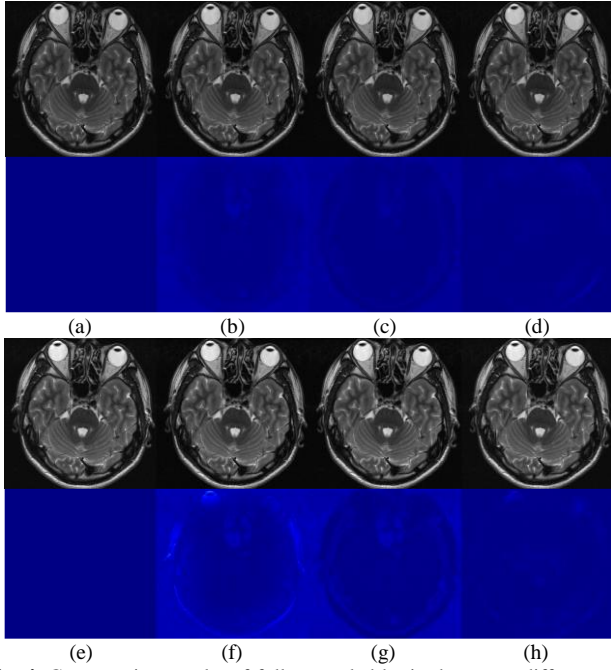


Fig. 4. Compression results of fully-sampled brain dataset at different virtual coils for different methods. Top: (a)(e) Reference image; (b) SCC-6ch;

(c) GCC-6ch; (d) VAN-ICC-I-6ch; (f) SCC-4ch; (g) GCC-4ch; (h) VAN-ICC-I-4ch. Bottom: The absolute difference images between the reference image and compression images.

3) **Reconstruction of Undersampled Data:** Since our model achieves excellent performance of coil compression on fully-sampled data, in this subsection we go a step further, i.e., we apply VAN-ICC-I to compress under-sampled images for accelerating imaging. More precisely, the under-sampled 20-coil cardiac datasets with Cartesian sampling and acceleration factor  $R=3$  are utilized as the network input to be compressed into 10-coil under-sampled images. Then the compressed images are transformed into k-space through Fourier transform. In addition, the compressed k-space data obtained by VAN-ICC-I, SCC, GCC and the original 20-coil under-sampled k-space data are all reconstructed by  $L_1$ -SPIRiT [47,48] algorithm.

Quantitative and qualitative evaluations are listed in Tab. 4 and Fig. 5., respectively. Fig. 5. (c) implies that the reconstruction results by  $L_1$ -SPIRiT with compressed images through SCC has large loss of details. Although GCC in Fig. 5. (d) has the excellent reconstruction quality, its performance is still worse than VAN-ICC-I in Fig. 5. (e). Table 3 provides the assessment values corresponding to different methods. The PSNR value of VAN-ICC-I is 32.32 dB and the SSIM value is 0.8676, which are both approaching to the result achieved by  $L_1$ -SPIRiT on 20-coils data. In brief, the proposed VAN-ICC-I is capable of fruitfully accelerating reconstruction, which has less errors in comparison with other compression methods.

TABLE III  
QUANTITATIVE RECONSTRUCTION RESULTS FOR VAN-ICC, SCC AND GCC ON  
THE UNDER-SAMPLED DATASET.

Dataset	20ch	SCC-10ch	GCC-10ch	VAN-ICC-10ch
Cardiac	32.49/ 0.8691	29.24/ 0.8652	31.43/ 0.8657	<b>32.32/ 0.8676</b>

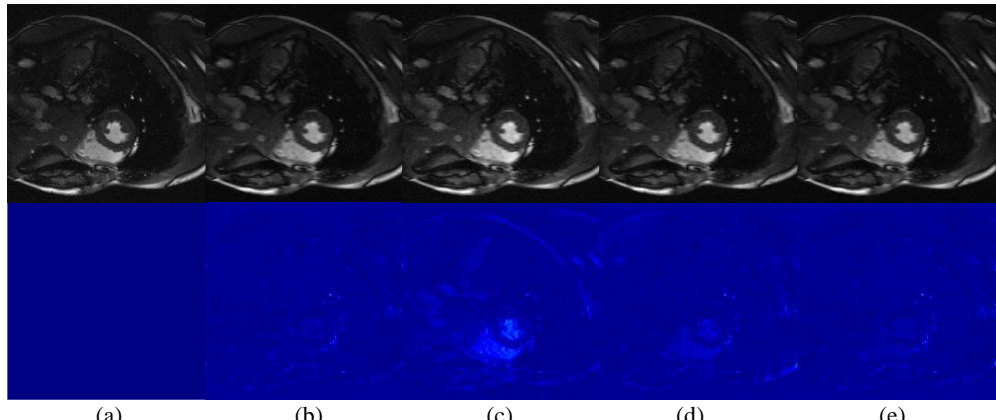


Fig. 5. Reconstruction results of under-sampled cardiac dataset for different methods. Top: (a) Reference image; (b)  $L_1$ -SPIRiT on 20-coils data; (c)  $L_1$ -SPIRiT on SCC-10ch data; (d)  $L_1$ -SPIRiT on GCC-10ch data; (e)  $L_1$ -SPIRiT on VAN-ICC-I-10ch. Bottom: The absolute difference images between the reference image and reconstruction images.

### C. Experiments on K-space Domain

1) **Coil Compression of Fully Sampled Data:** In contrast to previous experiments with fully sampled data on image domain, in this experiment brain data of 12 channels on k-space domain are compressed into 4 virtual coils and cardiac data of 20 channels on k-space domain are compressed into 10 virtual coils, respectively. Peak signal-to-noise ratio (PSNR) and structural similarity index (SSIM) are selected for quantitative assessments of reconstructed image quality in

Table IV. For the brain datasets, the PSNR value and SSIM value of VAN-ICC-K is able to be achieved as an excellent indicator. Among the methods, the results compressed by VAN-ICC-K have a good average PSNR value of 47.49 dB which is the highest. VAN-ICC-K also acquires an average SSIM value of 0.99, which performs well. For the cardiac datasets, the results compressed by VAN-ICC-K reaches a mean PSNR value of 40.86 dB, which is superior than SCC and GCC. This method has an average SSIM value of 0.9903, which is competitive of several compared with other meth-

ods.

TABLE IV  
QUANTITATIVE EVALUATION (PSNR/SSIM) RESULTS BY  
DIFFERENT METHODS IN THE TEST DATASETS.

Algorithm	SCC	GCC	VAN-ICC-K
Brain	41.37/0.9768	43.11/0.9786	<b>47.49/0.9936</b>
Cardiac	31.13/0.9758	36.59/ <b>0.9917</b>	<b>40.86/0.9903</b>

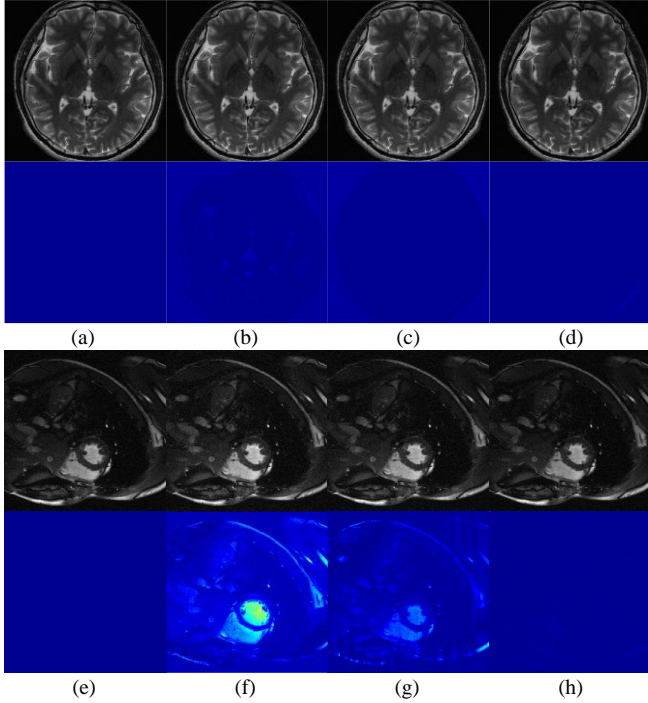


Fig. 6. Comparison of compression results on brain dataset and cardiac dataset for different methods. (top 2 rows: brain images, and bottom 2 rows: cardiac images) Top: (a) Reference image of brain dataset; (b) SCC-4ch; (c) GCC-4ch; (d) VAN-ICC-K-4ch; (e) Reference image of cardiac dataset; (f) SCC-10ch; (g) GCC-10ch; (h) VAN-ICC-K-10ch. Bottom: The  $2 \times$  absolute difference images between the reference images and compressed images of corresponding position.

The compression results are clearly presented in Fig. 6. The reference images are the SOS brain images of 12 original physical coils and the SOS cardiac images of 20 original physical coils. It is striking to observe that the images compressed by VAN-ICC-K have heavily slight loss and the quality of compression results is almost identical to the original images. In the meantime, the compressed results by VAN-ICC-K maintain features that preserve good imaging details and edge parts, so that the compression images with superb visual effects still retain as much intact and structural information as possible. It is commendably verified by the absolute difference map in Fig. 6.

2) *Compression for Different Virtual Coils*: The following experiment will validate the robustness of the previously introduced VAN-ICC-K. For better validation, the experiment chooses to compress the 12 original physical coils brain images into 3, 4, 5, and 6 virtual coils and compress the 20 original physical coils cardiac images into 4, 5, 8, and 10 virtual coils respectively. In general, the compression performance increases with the number of virtual coils in the same case, with a proportional relationship between these two variables. However, it is worth noting that the compression results obtained by the VAN-ICC-K method are not poor, as can be noticed in Fig. 7. The original images are able to retain most of the features incomparably when being compressed into 3 and 4 virtual coils. The quantitative results of this experiment are presented in detail in Table V. Compared to VAN-ICC-K, the average PSNR values for GCC and SCC are reduced by 8.09 dB and 6.12 dB, respectively when compressing the original image into 3 virtual coils and 4 virtual coils. In the same case, the average PSNR of VAN-ICC-K increases, making this algorithm undoubtedly optimal among the three in terms of compression performance.

TABLE V  
QUANTITATIVE RECONSTRUCTION RESULTS FOR VAN-ICC, SCC AND GCC AT DIFFERENT VIRTUAL COILS.

Dataset		SCC	GCC	VAN-ICC-K
Brain	12ch $\rightarrow$ 3ch	38.08/0.9763	41.36/0.9652	<b>46.17/0.9904</b>
	12ch $\rightarrow$ 4ch	41.37/0.9768	43.11/0.9786	<b>47.49/0.9936</b>
	12ch $\rightarrow$ 5ch	44.07/0.9869	45.74/0.9894	<b>48.71/0.9952</b>
	12ch $\rightarrow$ 6ch	45.83/0.9897	48.64/0.9951	<b>48.92/0.9952</b>
Cardiac	20ch $\rightarrow$ 4ch	29.88/0.9207	29.77/0.9327	<b>34.68/0.9557</b>
	20ch $\rightarrow$ 5ch	30.26/0.9379	31.47/0.9516	<b>35.13/0.9672</b>
	20ch $\rightarrow$ 8ch	30.87/0.9720	34.37/0.9820	<b>38.11/0.9822</b>
	20ch $\rightarrow$ 10ch	31.13/0.9758	36.59/ <b>0.9917</b>	<b>40.86/0.9903</b>

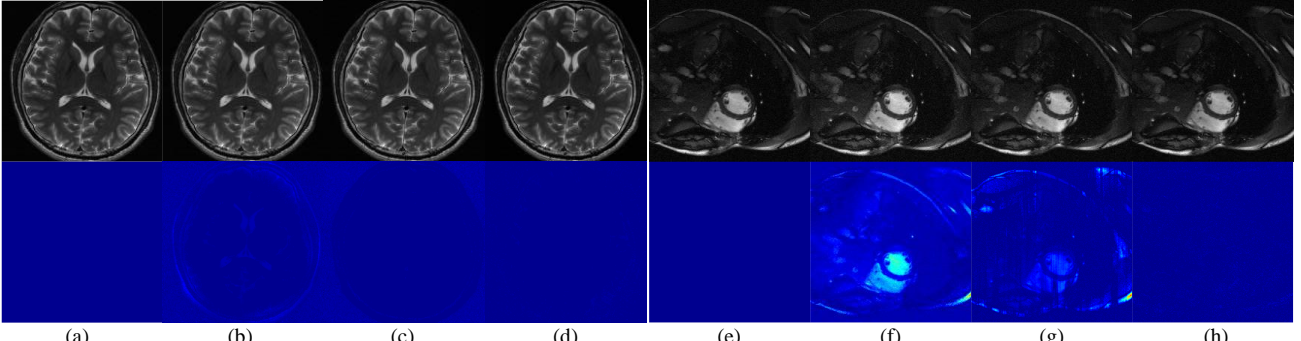


Fig. 7. Compression results of fully-sampled brain dataset at different virtual coils for different methods. (left 2 rows: brain images, and right 2 rows: cardiac images) (a) Reference image of brain dataset; (b) SCC-3ch; (c) GCC-3ch; (d) VAN-ICC-K-3ch; (f) SCC-8ch; (g) GCC-8ch; (h) VAN-ICC-K-8ch. Bottom: The  $2 \times$  absolute difference images between the reference images and compression images.

3) **Reconstruction of Under-sampled Data:** In this experiment, we will employ VAN-ICC-K to compress under-sampled images to speed up the imaging of the images. To put it in another concrete way, that is cartesian sampling of the cardiac datasets with an acceleration factor  $R = 3$ . In the first step, the 20-channel under-sampled cardiac MR images on k-space domain are compressed into 10-coil under-sampled images utilizing SCC, GCC and our proposed VAN-ICC-K methods. In the second and final step, the ESPIRiT [47] and  $L_1$ -SPIRiT [48] algorithms are used to reconstruct the compressed virtual coil images and original physical coil image. The reconstruction results are evaluated quantitatively. Table VI visualizes the experimental results, the average PSNR values of VAN-ICC-K are 30.30 dB for ESPIRiT algorithm and 30.87 dB for  $L_1$ -SPIRiT algorithm, which performs most graceful among the three algorithms. Particularly, the results with virtual coil images compressed by VAN-ICC-K are severely closed to the reconstruction results with original physical coil images. Under the same

circumstances, the average SSIM values of VAN-ICC-K are 0.7124 and 0.8104, which are higher than reconstruction results with virtual coil images by SCC and GCC. From Fig. 8, we can accurately find out that the VAN-ICC-K method is implemented to obtain reconstructed image effectively reduces blending artefacts compared with the GCC and SCC methods. In general, VAN-ICC-K has the advantage of minimizing the amount of data storage and computation of reconstruction with slight loss.

TABLE VI  
QUANTITATIVE RECONSTRUCTION RESULTS FOR VAN-ICC, SCC AND GCC ON THE UNDER-SAMPLED DATASET.

Dataset	20ch	SCC-10ch	GCC-10ch	VAN-ICC-10ch
ESPIRiT	26.70/0.567 8	24.61/0.509 2	25.75/0.526 6	<b>30.30/0.7124</b>
$L_1$ -SPIRiT	31.51/0.821 5	28.99/0.807 4	30.11/0.799 6	<b>30.87/0.8104</b>

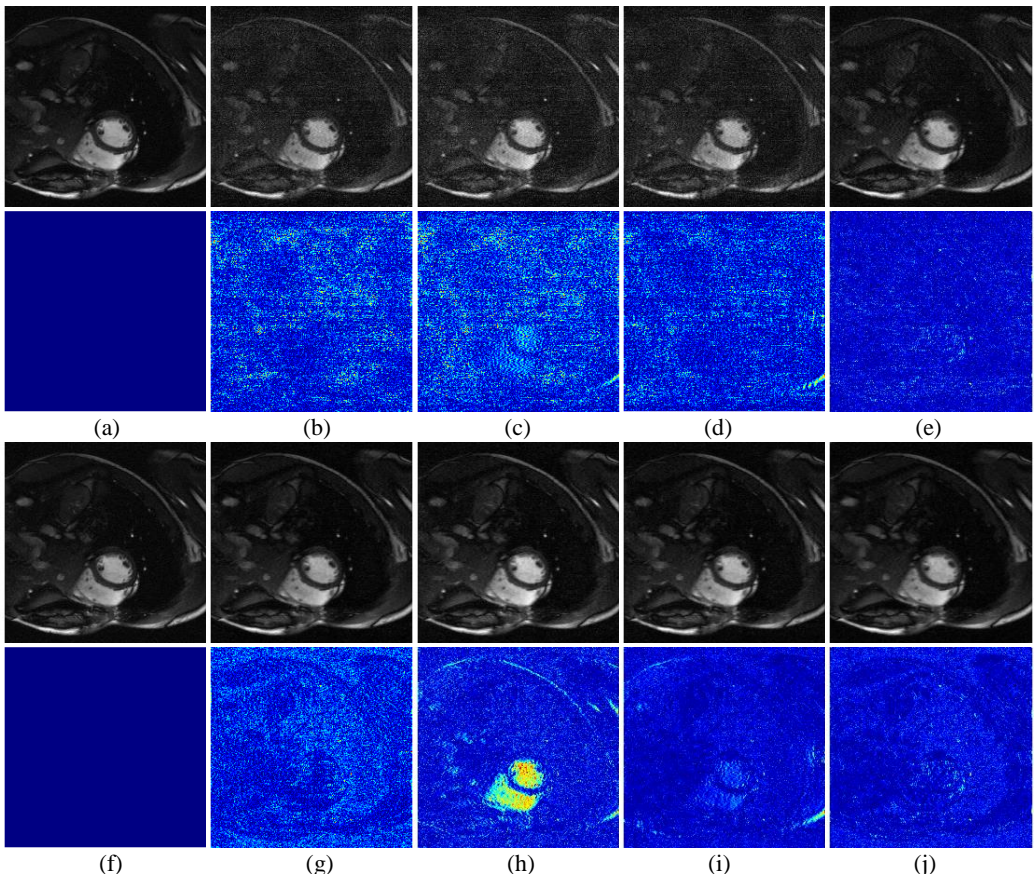


Fig. 8. Reconstruction results of under-sampled cardiac dataset for different methods. (top 2 rows: reconstruction results for ESPIRiT, and bottom 2 rows: reconstruction results for  $L_1$ -SPIRiT) Top: (a)(f) Reference image; (b) ESPIRiT on original 20-coils data; (c) ESPIRiT on SCC-10ch data; (d) ESPIRiT on GCC-10ch data; (e) ESPIRiT on VAN-ICC-K-10ch; (g)  $L_1$ -SPIRiT on original 20-coils data; (h)  $L_1$ -SPIRiT on SCC-10ch data; (i)  $L_1$ -SPIRiT on GCC-10ch data; (j)  $L_1$ -SPIRiT on VAN-ICC-K-10ch. Bottom: The  $3 \times$  absolute difference images between the reference image and reconstruction images.

4) **Time Cost of Compression and Reconstruction:** The greatest advantage of coil channel compression is that it reduces reconstruction time, thus we will evaluate the computing efficiency of the coil channel compression technique. The compression time and reconstruction time are the total time taken to process the data. The lower the total time, the more efficient the method. In this experiment, in the first step, we will make use of SCC, GCC and VAN-ICC-K to compress the brain datasets and cardiac datasets into the same virtual coil images. In the second step, the  $L_1$ -SPIRiT algorithm is utilized to reconstruct the compression results from the first

step. Obviously, during the first step time, our cost is compression time, which is presented in Table VII, and the other is reconstruction time demonstrated in Table VIII. And from these tables, the compression time and reconstruction time among SCC, GCC and VAN-ICC-K is barely analogous. Thus, it is not difficult to conclude that VAN-ICC-K efficiently reduces the computational time via compressing the physical coils before reconstructing them, which could help us to improve the computational efficiency and save the image reconstruction time.

TABLE VII  
QUANTITATIVE RESULTS FOR TIME COST OF COMPRESSION.

Algorithm	SCC	GCC	VAN-ICC-K
Brain	0.028s	0.157s	0.065s
Cardiac	0.042s	0.169s	0.058s

TABLE VIII  
QUANTITATIVE RESULTS FOR TIME COST OF  $L_1$ -SPIRiT RECONSTRUCTION.

Dataset	original	SCC	GCC	VAN-ICC-K
Brain	9.9618s	4.6525s	4.4172	4.4407s
Cardiac	10.2533s	5.9394s	6.1990s	5.9256s

**5) Reversible Recovery Fully Sampled Data:** To verify the reversibility of the model, the compressed images are taken as the input of the invertible network. By implementing the backward mapping, we can get the restored images with the same number of coils as the original images. The PSNR and SSIM values of the forward and backward processes on brain datasets are listed in Table IX. It is observed that PSNR values of the backward process exceed 120.68 dB on brain datasets.

Fig. 9 depicts the comparison results of reference images, compressed images and restored images. In comparison, backward process of the proposed VAN-ICC-K generates results that are much closer to the reference images. Overall, by qualitatively and quantitatively comparing the restored results, it can be observed that VAN-ICC-K is able to perform reversible operations on the compressed images, which is not possible for other traditional coil compression methods.

TABLE IX  
QUANTITATIVE EXPANSION (PSNR/SSIM) RESULTS FOR VAN-ICC-K  
AT DIFFERENT VIRTUAL COILS.

Dataset	Forward process	Backward process
Brain	48.73/0.9945	120.68/0.9999

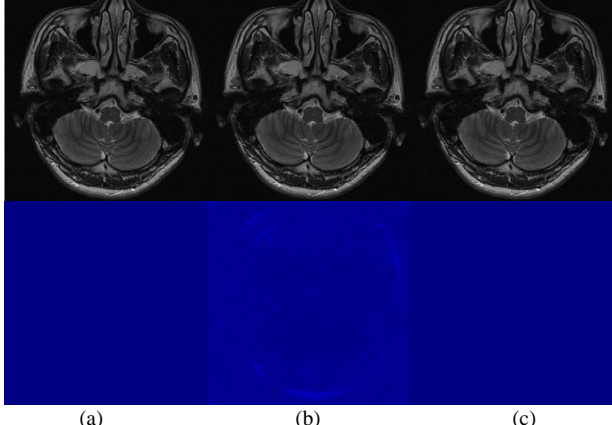


Fig. 9. Reversible recovery results of Brain dataset for VAN-ICC-K. Top: (a) Reference image of brain dataset; (b) VAN-ICC-K-6ch; (c) Recovery images by VAN-ICC-K. Bottom: The 5  $\times$  absolute difference images between the reference image and compression and recovery images.

## V. CONCLUSIONS

In this paper, we introduced a novel deep learning-based invertible model VAN-ICC-K for compressing coils. The employed method is inspired by invertible neural networks. Auxiliary variables technology is adopted to implicitly reduce the dimension of coils. Therefore, the model is able to not only compress the multi-coils data, but also recover the compressed image reversibly, which alleviates the burden of data storage and reconstruction time. Experiments indicated that the raised VAN-ICC-K method outperforms conven-

tional SCC and GCC approaches, exhibiting potentials in both research and clinical settings.

## REFERENCES

- [1] K. P. Pruessman, M. Weiger, M. B. Scheidegger, and P. Boesiger, "SENSE: Sensitivity encoding for fast MRI," *Magn. Reson. Med.*, vol. 42, no. 5, pp. 952-962, 1999.
- [2] M. A. Griswold, P. M. Jakob, R. M. Heidemann, M. Nittka, V. Jellus, J. Wang, B. Kiefer, and A. Haase, "Generalized autocalibrating partially parallel acquisitions (GRAPPA)," *Magn. Reson. Med.*, vol. 47, no. 6, pp. 1202-1210, 2002.
- [3] T. Zhang, J. M. Pauly, S. S. Vasanawala, and M. Lustig, "Coil compression for accelerated imaging with Cartesian sampling," *Magn. Reson. Med.*, vol. 69, no. 2, pp. 571-582, 2013.
- [4] M. A. Ohliger, and D. K. Sodickson, "An introduction to coil array design for parallel MRI," *NMR Biomed.*, vol. 19, no. 3, pp. 300-315, 2006.
- [5] K. Nael, M. Fenchel, M. Krishnam, G. Laub, J. P. Finn, and S. G. Ruehm, "High-spatial-resolution whole-body MR angiography with high-acceleration parallel acquisition and 32-channel 3.0-T unit: initial experience," *Radiology*, vol. 242, no. 3, pp. 865-872, 2007.
- [6] M. A. Hernandes, R. C. Semelka, J. Elias Júnior, S. Bamrungrachart, B. M. Dale, and C. Stallings, "Whole-body MRI: comprehensive evaluation on a 48-channel 3T MRI system in less than 40 minutes. Preliminary results," *Radiologia Brasileira*, vol. 45, no. 6, pp. 319-325, 2012.
- [7] C. J. Hardy, R. O. Giaquinto, J. E. Piel, K. W. Rohling, L. Marinelli, D. J. Blezek, E. W. Fiveland, R. D. Darrow, and T. K. F. Foo, "128-channel body MRI with a flexible high-density receiver-coil array," *J. Magn. Reson. Imaging*, vol. 28, no. 5, pp. 1219-1225, 2008.
- [8] F. Huang, S. Vijayakumar, Y. Li, S. Hertel, and G. R. Duensing, "A software channel compression technique for faster reconstruction with many channels," *Magn. Reson. Imaging*, vol. 26, no. 1, pp. 133-141, 2008.
- [9] M. Buehrer, K. P. Pruessmann, P. Boesiger, and S. Kozerke, "Array compression for MRI with large coil arrays," *Magn. Reson. Med.*, vol. 57, no. 6, pp. 1131-1139, 2007.
- [10] M. Doneva, and P. Börnert, "Automatic coil selection for channel reduction in SENSE-based parallel imaging," *Magn. Reson. Mat. Phys. Biol. Med.*, vol. 21, no. 3, pp. 187-196, 2008.
- [11] S. B. King, S. M. Varosi, and G. R. Duensing, "Optimum SNR data compression in hardware using an Eigen-coil array," *Magn. Reson. Med.*, vol. 63, no. 5, pp. 1346-1356, 2010.
- [12] S. B. King, S. M. Varosi, F. Huang, and G. R. Duensing, "The MRI eigencoil: 2N-channel SNR with N-receivers," *Proc. 11th Annual Meeting of the International Society for Magnetic Resonance in Medicine*, vol. 712, 2003.
- [13] M. Ringnér, "What is principal component analysis?," *Nat. Biotechnol.*, vol. 26, no. 3, pp. 303-304, 2008.
- [14] G. Destefanis, M. T. Barge, A. Brugia, and S. Tassone, "The use of principal component analysis (PCA) to characterize beef," *Meat Sci.*, vol. 56, no. 3, pp. 255-259, 2000.
- [15] S. Karamizadeh, S. M. Abdullah, A. A. Manaf, M. Zamani, and A. Hooman, "An overview of principal component analysis," *Journal of Signal and Information Processing*, vol. 4, no. 3B, pp. 173-175, 2013.
- [16] S. Feng, Y. Zhu, and J. Ji, "Efficient large-array k-domain parallel MRI using chan-nel-by-channel array reduction," *Magn. Reson. Imaging*, vol. 29, no. 2, pp. 209-215, 2011.
- [17] P. J. Batty, S. Chang, J. H. Holmes, K. Wang, A. C. S. Brau, S. B. Reeder, and J. H. Brittain, "Design of k-space channel combination kernels and integration with parallel imaging," *Magn. Reson. Med.*, vol. 71, no. 6, pp. 2139-2154, 2014.
- [18] A. Radford, L. Metz, and S. Chintala, "Unsupervised representation learning with deep convolutional generative adversarial networks," *arXiv preprint, arXiv:1511.06434*, 2015.
- [19] A. Grover, M. Dhar, and S. Ermon, "Flow-gan: Combining maximum likelihood and adversarial learning in generative models," *Thirty-second AAAI conference on artificial intelligence*, 2018.
- [20] D. P. Kingma, and J. Ba, "Adam: A method for stochastic optimization," *arXiv preprint, arXiv:1412.6980*, 2014.
- [21] L. Dinh, J. Sohl-Dickstein, and S. Bengio, "Density estimation using real nvp," *arXiv preprint, arXiv:1605.08803*, 2016.
- [22] D. P. Kingma, and P. Dhariwal, "Glow: generative flow with invertible 1x1 convolutions," *arXiv preprint, arXiv:1807.03039*, 2018.
- [23] L. Dinh, D. Krueger, and Y. Bengio, "Nice: Non-linear independent components estimation," *arXiv preprint, arXiv: 1410.8516*, 2014.
- [24] J. Ho, X. Chen, A. Srinivas, Y. Duan, and P. Abbeel, "Flow++: Improving flow-based generative models with variational dequantiza-

tion and architecture design,” *International Conference on Machine Learning. PMLR*, pp. 2722-2730, 2019.

[25] M. Xia, X. Liu, and T Wong, “Invertible grayscale,” *ACM Trans. Graph.*, vol. 37, no. 6, pp. 1-10, 2018.

[26] C. Chen, Q. Chen, J. Xu, and V. Koltun, “Learning to see in the dark,” *Proceedings of the IEEE Conference on Computer Vision and Pattern Recognition*, pp. 3291-3300, 2018.

[27] S. Ioffe, and C. Szegedy, “Batch normalization: Accelerating deep network training by re-ducing internal covariate shift,” *International conference on machine learning. PMLR*, pp. 448-456, 2015.

[28] Q. Liu, and H. Leung, “Variable augmented neural network for de-colorization and multi-exposure fusion,” *Inf. Fusion*, vol. 46, pp. 114-127, 2019.

[29] P. Jaini, K. A. Selby, and Y. Yu, “Sum-of-squares polynomial flow,” *International Conference on Machine Learning. PMLR*, pp. 3009-3018, 2019.

[30] S. Prajna, A. Papachristodoulou, and P. A. Parrilo, “Introducing SOSTOOLS: A general purpose sum of squares programming solver,” *Proceedings of the 41st IEEE Conference on Decision and Control*, vol. 1, pp. 741-746, 2002.

[31] K. Tanaka, H. Yoshida, H. Otake, and H. O. Wang, “A sum-of-squares approach to modeling and control of non-linear dynamical systems with polynomial fuzzy systems,” *IEEE Trans. Fuzzy Syst.*, vol. 17, no. 4, pp. 911-922, 2008.

[32] A. Grover, M. Dhar, and S. Ermon, “Flow-gan: Combining maximum likelihood and adversarial learning in generative models,” *Thirty-second AAAI conference on artificial intelligence*, 2018.

[33] F. Zhang, X. Xu, Z. Xiao, J. Wu, L. Geng, W. Wang, and Y. Liu, “Automated quality classification of colour fundus images based on a modified residual dense block network,” *Signal, Image and Video Processing*, vol. 14, no. 1, pp. 215-223, 2020.

[34] A. F. Agarap, “Deep learning using rectified linear units (relu),” *arXiv preprint, arXiv: 1803.08375*, 2018.

[35] L. Weng, H. Zhang, H. Chen, Z. Song, C. Hsieh, L. Daniel, D. Boning, and I. Dhillon, “Towards fast computation of certified robustness for relu networks,” *International Conference on Machine Learning. PMLR*, pp. 5276-5285, 2018.

[36] D. Zou, Y. Cao, D. Zhou, and Q. Gu, “Gradient descent optimizes over-parameterized deep ReLU networks,” *Mach. Learn.*, vol. 109, no. 3, pp. 467-492, 2020.

[37] B. Xu, N. Wang, T. Chen, and M. Li, “Empirical evaluation of rectified activations in convolutional network,” *arXiv preprint, arXiv: 1505.00853*, 2015.

[38] Y. Liu, X. Wang, L. Wang, and D. Liu, “A modified leaky ReLU scheme (MLRS) for topology optimi-zation with multiple materials,” *Appl. Math. Comput.*, vol. 352, pp. 188-204, 2019.

[39] J. Xu, Z. Li, B. Du, M. Zhang, and J. Liu, “Reluplex made more practical: Leaky ReLU,” *ISCC*, pp. 1-7, 2020.

[40] G. R. Lee, R. Gommers, F. Waselewski, K. Wohlfahrt, and A. O’Leary, “PyWavelets: A Python package for wavelet analysis,” *Journal of Open Source Software*, vol. 4, no. 36, pp. 1237, 2019.

[41] A. Horé, and D. Ziou, “Image quality metrics: PSNR vs. SSIM,” *2010 20th international conference on pattern recognition*, pp. 2366-2369, 2010.

[42] Q. Huynh-Thu, and M. Ghanbari, “Scope of validity of PSNR in image/video quality assessment,” *Electron. Lett.*, vol. 44, no. 13, pp. 800-801, 2008.

[43] D. Lenyel, D. Kalen, and S. Wolf, “US Coast Guard High Frequency Emergency Network (HFEN) implementation plan,” *NASA STI/Recon Technical Report N*, vol. 85, pp. 29141, 1985.

[44] Z. Chen, H. Lu, S. Tian, J. Qiu, T. Kamiya, S. Serikawa, and L. Xu, “Construction of a hierarchical feature enhancement network and its application in fault recognition,” *IEEE Trans. Ind. Inform.*, vol. 17, no. 7, pp. 4827-4836, 2020.

[45] S. Ravishankar, and Y. Bresler, “MR image reconstruction from highly undersampled k-space data by dictionary learning,” *IEEE Trans. Ind. Inform.*, vol. 30, no. 5, pp. 1028-1041, 2010.

[46] S. G. Lingala, and M. Jacob, “Blind compressive sensing dy-namic MRI,” *IEEE Trans. Med. Imaging*, vol. 32, no. 6, pp. 1132-1145, 2013.

[47] M. Lustig, and J. M. Pauly, “SPIRiT: Iterative self-consistent parallel imaging reconstruction from arbitrary k-space,” *Magn. Reson. Med.*, vol.64, no. 2, pp. 457-471, 2010.

[48] M. Murphy, K. Keutzer, S. Vasanawala, and M. Lustig, “Clinically feasible reconstruction time for L1-SPIRiT parallel imaging and compressed sensing MRI,” *In Proceedings of the ISMRM Scientific Meeting & Exhibition*, vol. 4854, 2010.